Changing circulation structure and precipitation characteristics in Asian monsoon regions: greenhouse warming vs. aerosol effects

William K.M. Lau[1,2] Kyu-Myong Kim[3] and L. Ruby Leung[4]

[1] *Earth System Science Interdisciplinary Center, U. of Maryland*

[2] *Department of Atmospheric and Oceanic Sciences, U. of Maryland*

College Park, MD 20740

[3] *Climate and Radiation Laboratory, NASA/Goddard Space Flight Center*

Greenbelt, MD 20771

[4]*Pacific Northwest National Laboratory, Richland, Washington, 99352*

August 2017

Submitted to Geoscience Letters

William K. M.Lau <wkmlau@umd.edu>

Kyu-Myong Kim <Kyu-Myong.Kim@nasa.gov>

Ruby Leung <ruby.leung@pnnl.gov>

Abstract

Using model outputs from CMIP5 historical integrations, we have investigated the relative roles of anthropogenic emissions of greenhouse gases (GHG) and aerosols in changing the characteristics of the large-scale circulation and rainfall in Asian summer monsoon (ASM) regions. Under GHG warming, a strong positive trend in low-level moist static energy (MSE) is found over ASM regions, associated with increasing large-scale land-sea thermal contrast from 1870's to present. During the same period, a mid-tropospheric convective barrier (MCB) due to widespread reduction in relative humidity in the mid- and lower troposphere is strengthening over the ASM regions, in conjunction with expanding areas of anomalous subsidence associated with the Deep Tropical Squeeze (DTS) [Lau and Kim, 2015]. The opposing effects of MSE and MCB lead to enhanced total ASM rainfall, but only a partial strengthening of the southern portion of the monsoon meridional circulation, coupled to anomalous multi-cellar overturning motions over ASM land. Including anthropogenic aerosol emissions strongly masks MSE but enhances MCB via increased stability in the lower troposphere, resulting in an overall weakened ASM circulation with suppressed rainfall. Rainfall characteristics analyses indicate that under GHG, overall precipitation efficiency over the ASM region is reduced, manifesting in less moderate but more extreme heavy rain events. Under combined effects of GHG and aerosols, precipitation efficiency is unchanged, with more moderate, but less extreme rainfall.

1. Introduction

Despite the large number of recent studies, the relative roles of anthropogenic greenhouse warming vs. aerosols on Asian monsoon (ASM) climate change remain mired as a subject of debate and continued intense research (Ramanathan et al. 2001, Chung and Ramanathan 2006, Lau et al. 2006, 2008, Meehl et al. 2008, Ramanathan and Carmichael 2008, Wang et al. 2009, Li et al., 2010, Bollasina et al. 2011, Lee and Wang 2012, Turner and Annamalai 2012, Wang et al. 2012, IPCC 2013, Krishnan et al. 2013, Song et al. 2014, Li et al. 2016, Jin and Wang 2017, and many others). One of the main reasons for the slow progress is that ASM climate change is an immensely complex phenomenon, involving global scale forcing, coupled to regional and local scale feedbacks arising from natural variability in the atmosphere-ocean-land system, as well as human activities. Another is the imperative to understand climate impacts such as droughts and floods on local and human scales, where application of climate model results are deficient, due to limitations of resolution and inadequate physical process representation. This is particularly true for ASM modeling, where even the simulation skills of seasonal climatology and intraseasonal variability of rainfall are still wanting [Webster et al. 1998, Wang 2006, Lau and Waliser 2012, and Sperber et al. 2013, Ashfaq et al. 2016].

On the other hand, CMIP (Coupled Model Intercomparison Project) ensemble climate models have provided significant advance in understanding the thermodynamic and dynamical effects of greenhouse warming on circulation, temperature, moisture, rainfall pattern consistent with the basic governing principles of the ocean-atmosphere general circulations [Held and Soden 2006, Vecchi and Soden 2007, Xie et al. 2009, Sherwood et al. 2010, Tokinaga et al. 2012, Santer et al., 2012, Lau et al. 2013, Lau and Kim

70 2015]. These global scale changes will undoubtedly have impacts on key monsoon drivers,
71 *e.g.,* sea surface temperature, hemispheric and land-sea thermal contrasts, regional moist
72 static energy, and tropospheric relative humidity [Fasullo 2012, Murugavel et al. 2012,
73 Roxy et al. 2015, Li et al. 2015, Zhang and Li 2016]. Knowing the impacts of greenhouse
74 warming vs. aerosols on these monsoon drivers will provide better understanding at a
75 more fundamental level, of their roles in affecting structural changes (shifting, deepening,
76 narrowing and widening) in the monsoon regional circulation and in characteristics
77 (types, duration, and intensity) of monsoon rainfall. Provided statistics are taken with
78 multi-model ensembles, and over large-scale domain*, e.g.,* the entire Asian monsoon, or
79 sub-continental domains (South Asia or East Asia), as opposed to local (human) scales,
80 climate models have higher fidelity to the real world. This is not to say that the human
81 scales are unimportant, but rather focusing on global and regional scale forcing and
82 response will provide an intermediate step, where climate models can be used to inform
83 downscaling studies to better understand ASM climate change on human scales [Fowler et
84 al., 2007].

85 Using the aforementioned approach, Lau and Kim [2017], hereafter referred to as
86 LK, studied the competing influences of greenhouse warming vs. aerosols on Asian
87 monsoon climate. LK identified under a historical GHG-only warming scenario, an
88 increasing land-sea temperature difference between 5^{o} S to 30^{o} N since the 1950's, dubbed
89 the Warm-Ocean-Warmer-Land (WOWL) effect, as a primary driver of the ASM climate
90 change, enhancing moisture transport from ocean to the ASM land, including strong cross-
91 equatorial transport of moisture via the Somali jet, from the colder (southern) to the
92 warmer (northern) hemisphere. They found that GHG also induces an increase in mid-

93 tropospheric dryness which acts as a barrier to deep convection, suppressing monsoon
94 rainfall over ASM regions. Furthermore, a warmer upper troposphere over the Indo-
95 Pacific warm pool under global warming tends to inhibit the northward advance of the
96 ASM. The net result is that under GHG, while the overall ASM rainfall is increased, the
97 monsoon meridional circulation (MMC) is weakened. LK found that aerosols strongly
98 mask the GHG effects, reducing the WOWL effect by 50-60 %. Additionally, aerosols
99 increase atmospheric stability over ASM land region, alluding to the presence of a
100 convective barrier, which may cause further suppress monsoon rainfall and weaken the
101 MMC. This paper is an extension of LK to further elucidate the GHG vs. aerosol impacts
102 on monsoon circulation structure and rainfall characteristics. Specifically, we investigate
103 the possible effects of a mid-level convective barrier, associated with structural changes in the
104 Asian MMC under GHG, and modulation by anthropogenic aerosol forcing. Possible
105 relationship of the convective barrier to the changing nature of precipitation under GHG and
106 under the combined effects of GHG and aerosol forcing will also be investigated.

107 **2. Methodology and data**

108 We used outputs from 135 year historical simulations (1870- 2005) of 19 CMIP5
109 coupled models, with prescribed anthropogenic emissions of a) greenhouse gases (GHG)
110 only and b) GHG and aerosols (All). Each model is integrated starting from its own
111 equilibrium pre-industrial climate. All model outputs have been interpolated to a
112 common grid of 2.5 x 2.5 latitude-longitude. To focus on the forced response of the ASM to
113 anthropogenic emission forcing, we minimize the impacts of natural variability by
114 constructing the Multi-Model mean (MMM) of all key quantities for the boreal summer
115 season (June-July-August). Anomalies are defined as the last 25 years (1981-2005),

116 relative to pre-industrial equilibrium climate. The MMM anomalies of the GHG
117 integrations will be used to establish the baseline for the ASM climate forcing and
118 response. By comparing ALL to GHG, the extent to which GHG-induced anomalies are
119 modulated by aerosols will be assessed. Changes in rainfall characteristics will be
120 explored using scale analysis based on water balance requirement [Sugiyama et al. 2010,
121 Lu et al., 2014], and quantile regression analysis [Buchinsky 1998, Lau and Wu 2006,
122 2011], as well as compared observations from APHRODITE [Yatagai et al. 2012].
123
124 **3. Results**
125 We first examine the global scale forcing of the ASM, from the perspective of changes
126 of the global mid-tropospheric vertical motions. Under GHG, the distribution of mean and
127 anomalous vertical motions at 500 hPa (Fig. 1a) shows anomalous ascent over the
128 equatorial central Pacific, and an intensification on the equatorward flank of the Inter-
129 Tropical Convergence Zone (ITCZ) in the eastern Pacific. As shown in LK, this is the boreal
130 summer manifestation of the Deep Tropical Squeeze (DTS) – a narrowing and
131 intensification of deep convective zone over the equatorial central and eastern Pacific
132 (region marked by the red-lined rectangle in Fig. 1a), in conjunction with a widening of the
133 subsiding branch of the Hadley Circulation (HC), under global warming [Lu et al. 2007,
134 Seidel et al. 2008, Hu et al. 2011, and Lau and Kim 2015]. Elsewhere, anomalous
135 subsiding motions are found over extensive areas in the tropics and subtropics, most
136 pronounced over land regions of Asia, the Maritime continent, and the North
137 American/Mexico monsoon regions and subtropical belt (35-40^{o}S) of the Southern
138 Hemisphere. Comparing to the climatology, changes within 5^{o}S- 20^{o}N signal a weakened

139 Walker Circulation (WC), while the anomalous subsidence poleward of 30° N mostly over
140 land in the Northern Hemisphere and near 35°S in the Southern Hemisphere reflect a
141 widening of the subsiding zone of the HC. The extensive subsidence regions coincide with
142 regions of reduced mid-tropospheric relative humidity [Lau and Kim 2015]. Under ALL,
143 the anomalous vertical motion pattern (Fig. 1b) is similar on the global scale, but
144 substantially weaker than GHG, with less tight gradients, except over the ASM domain
145 (marked by the box outlined in black in Fig. 1a), where the regions of anomalous descent
146 area have expanded.

147 The inverse relationship between the anomalous vertical motion over the ASM and
148 the DTS domain (box outlined in red) can be seen in the time series plots of area mean p-
149 velocity over each domain. Fig. 1c shows that the mid-tropospheric anomalous ascent
150 has been trending positive in the DTS region since the 1930's, with faster rate under GHG
151 compared to ALL, reflecting the aerosol masking effect [Ramanathan and Feng 2008, and
152 LK]. During the same period, the anomalous vertical motion have been trending negative
153 over the ASM domain, but with a faster rate under ALL than GHG (Fig. 1d). The changes
154 in the vertical motion in the two regions signal a weakening of the climatological WC
155 under GHG warming [Vecchi and Soden 2007, Tokinaga et al. 2012, and LK]. Under ALL, a
156 "masked" anomalous ascent over the DTS would have led to "weakened" anomalous
157 descent over the ASM, if the WC were the only dominant driver of the ASM Apparently,
158 this is *not* the case. Over ASM land region, cooling of the land surface by attenuation of
159 solar radiation by aerosols can lead to a spin-down of the ASM circulation [Ramanathan et
160 al., 2001]. Furthermore, the presence of abundant absorbing aerosols (BC, OC and dust) in
161 monsoon regions increases stability in the lower troposphere by warming above and

cooling near the surface [Menon et al. 2002, Lau et al., 2006, 2008, 2016, Fan et al. 2008, Wang et al., 2013]. These aerosol effects result in substantial "masking" of the Warm-Ocean-Warmer-Land (WOWL) effect, resulting in weakened anomalous moisture transport from ocean to monsoon land under ALL compared to GHG [See LK for details].

3.1 Regional monsoon controls

In this subsection, we examine changes in two major controls of the ASM, *i.e.*, low-level moist static energy (MSE) and mid-tropospheric relative humidity (ΔRH). Under GHG, an increasing potential for deep convection and precipitation is evidenced in a positive trend in ASM domain averaged (MSE) since 1950-1960's (Fig. 2a). This trend is almost identical to, and can identified with the WOWL effect (See Fig. 1 in LK) of increasing land-sea temperature contrast and moisture transport from ocean to ASM land. Under ALL, the MSE positive trend is substantially weakened, with the aerosol masking nearly 50-60 % of GHG trend in the 1960-2000's, reflecting the large increase in aerosol emissions, due to the rapid modernization taking place over Asia during this period. Contemporaneously, a "mid-tropospheric convective barrier" (MCB) represented by decreasing trend in mid-tropospheric RH can be seen under both GHG and ALL (Fig. 2b) since the early 1900's. The negative trends stem from moist adiabatic lapse-rate feedback and remote forcing from anomalous subsidence associated with the DTS under GHG warming (see LK for details). Briefly, warm moist air parcel ascending from low levels via the moist adiabatic will conserve moist static energy and experience larger warming in the upper and mid-troposphere relative to the lower troposphere. Based on the differential form of the Clausius Claypeyron equation relating to relative humidity R_h, *i.e.*, $\delta R_h = \delta q / q_s - \alpha R_h \delta T$, where $\alpha = L(R_v T^2)^{-1} \sim 6\% K^{-1}$, q, T represents the ambient specific

185 humidity and temperature respectively, and q_s the saturated humidity, it can be seen that
186 an increase in δT in the mid- and upper troposphere larger than $\delta q / q_s$ due to vertical
187 transport can lead to a reduction in R_h, *i.e.,* drying. Additionally, drier air from above
188 transported by anomalous downward motion under GHG remote forcing over the ASM
189 domain (See Fig. 1) can further dry the mid- and lower troposphere. The presence of the
190 MCB tends to inhibit deep convection, suppress rainfall, and limits the upward transport
191 of moisture locally, providing a positive feedback to the remote forcing. During the later
192 period (1970-2000's), the MCB is actually stronger (more negative RH) under ALL
193 compared to GHG as a result of aerosol effects in increasing atmospheric stability in the
194 mid- and lower troposphere, and limiting deep convection [Fan et al 2008, Wang et al
195 2013].
196 *3.2 Monsoon Meridional Circulation (MMC)*
197 In this subsection, MMC anomalies over the ASM are examined in relationship to
198 changes in LMSE, MCB, and rainfall (Fig. 3). Under GHG warming, the MMC shows
199 alternating anomalous ascent and descent over the ASM domain. The influence of the
200 anomalous Walker Circulation can be seen in the strong anomalous descent near 5^{o}S, and
201 moderate descent near 10^o N (Fig 3a, see also Fig. 1a). Poleward of 30^{o}N and S,
202 anomalous subsidence reflects the expansion of the subtropical subsidence zone of the HC,
203 in association with the DTS [Lau and Kim 2015, and LK]. While the increased MSE over
204 monsoon land enhances convective potential, deep convection with ascent throughout the
205 troposphere can only break out where it can overcome the MCB (Fig 3b). Judging from
206 the distribution of the anomaly relative to the climatological mean vertical motions, GHG
207 warming appears to have produced only limited enhancement of the ascending motions

over the ASM land, as evident in the alternating descent and ascent north of 10° N. On the other hand, the descent branch appears to have deepened and widened, with enhanced subsidence near 40°S, but weakened near the climatological descending center (20-30°S). Consistent with the vertical motion changes, rainfall is enhanced (decreased) in the climatological rising (sinking branch) of the MMC, with rates commensurate with a steady rise in LMSE from ocean to land, against the opposing tendency by the MCB *(*mid-tropospheric drying) across the MMC. This is particularly noteworthy, over the ASM land in subtropical and higher latitudes, where precipitation increase is only moderate (Fig. 3b). Under ALL (Fig. 3c, d), inclusion of aerosols leads to an overall weakened MMC, accentuating regions of anomalous subsidence under GHG warming over the ASM land domain (10-30° N). ASM rainfall is suppressed in conjunction with a muted increase in MSE, but increased MCB (negative ΔRH) over ASM land (10-30°N) compared to GHG.

3.3 Changing rainfall characteristics

Previous studies have shown that changes in rainfall characteristics can better reveal the underlying physical processes associated with climate change [Trenberth et al. 2003, Lau and Wu 2006, 2011, and Lau et al. 2013]. In this subsection, we evaluate the impacts of GHG and aerosols on rainfall characteristics in ASM region, in association with the changing MMC. Specifically, we will focus on changes in precipitation efficiency and rainfall types. Here, the change in precipitation efficiency will be examined via a scale analysis, based on the water balance requirements [Sugiyama et al. 2010, Lu et al 2014]. In ASM regions, where the climatological mean vertical motion is upward, the area mean precipitation P, can be expressed as

$$P = \alpha M q, \qquad (1)$$

where M=upward mass flux at cloud base, q=specific humidity at cloud base, and α is a scale factor representing the bulk precipitation efficiency, defined as rainfall per unit moisture flux at cloud base. As defined, α is dependent on the cloud properties and types, entrainment rate, and relative humidity of the environment [Li et al., 2002, Sui et al. 2007]. Differentiating Eq (1) yields

$$\frac{dP}{P} = \frac{dw}{w} + \frac{dq}{q} + \frac{d\alpha}{\alpha} \qquad (2)$$

where we have assumed that $\frac{dM}{M} \sim \frac{dw}{w}$, with w representing the vertical motion at 500 hPa level, which signifies the strength of the MMC. Since cloud base information for each CMIP5 model is not available, the approximation of cloud mass flux by vertical moisture flux at the mid- and lower troposphere has been used in many previous climate-scale rainfall scale analysis (Held and Soden 2006, Sugiyama et al. 2010, and Lu et al. 2014). The fractional change of area mean values of *P, w, q* for each simulated year from 1870-2005 (Fig. 4a) is computed relative to the pre-industrial climatology. Under GHG, the trend in increasing *q* is very pronounced, since the 1930's to 2005 (Fig. 4a). During the same period, the trend in increased rainfall is also obvious, but relatively muted relative to *q*, while the MMC shows a weakening (negative) trend, with magnitude comparable to but opposed to the rainfall. As a result, α shows a strong decreasing trend, signaling a large reduction in precipitation efficiency. Under ALL, the increasing trend in *q* is strong from 1960's to 2005, although weaker compared to GHG. Here, both rainfall and MMC show negative trends, with much faster rate in the latter, indicating a substantially weakened MMC with reduced overall ASM rainfall (see Fig. 3d). Interestingly, the bulk precipitation efficiency shows no noticeable trend during the last three decades, compared to GHG.

253 To investigate changes in precipitation types under GHG and ALL, following
254 previous work [Lau and Wu 2006, 2011], we have computed the model rainfall probability
255 distribution functions (pdf) over ASM land region and compared with observations from
256 APHRODITE [Yatagai et al. 2012]. Rainfall pdf's, binned by ranked rain rates, were first
257 constructed, over the ASM domain for the climatology. Twenty percentiles, with a bin
258 width of 5% were chosen, with the top 95% representing the most extreme rain events,
259 and the bottom 5%, the extreme light events*, i.e.*, drizzles. Quantile regression analysis
260 [Koenker 2005, Lau et al. 2013] was then carried out to extract the linear trend for each
261 percentile for the period 1950-2005. Under GHG (Fig. 5a), the probability of heavy rain
262 event (top 80%) is strongly increased, with the highest rate for the more extreme events.
263 However, moderate and light rain events are generally suppressed. In contrast under All
264 (Fig. 5b), the frequency of heavy rain (top 70%) is reduced, but moderate rain event
265 occurs more often, in good agreement with observations (Fig.5c). The physical reasons
266 for changing rainfall types under GHG and ALL are not obvious. Here, we offer a plausible
267 explanation, inferred from information currently available. Under GHG, over the ASM
268 domain, a given moist parcel rising from cloud base will lose cloud liquid mass by dry
269 detrainment as it encounters drier air in the MCB, and thus yield less precipitation per unit
270 moisture flux at cloud base, *i.e.*, reduction in bulk precipitation efficiency, consistent with
271 the reduction in moderate and light rain events. However, the steady increase in MSE due
272 to strong WOWL effect under GHG allows the build-up of excessive convective available
273 potential energy (CAPE) in the lower troposphere. Eventually, delayed deep convection
274 breaks out locally under conditions of locally forced strong upward motion, releasing the
275 excessive CAPE in the form of extreme heavy precipitation [Wang and Zhou 2005,

O'Gorman and Schneider 2009]. Under ALL, the "WOWL" effect is strongly "masked", resulting in a much slower rate of CAPE increase. In addition, the increased stability in the lower troposphere by aerosols sustains and strengthens the MCB, allowing only increase moderate rain, while suppressing extreme heavy rain [Fan et al. 2008, Yang et al. 2013]. The aforementioned scenario needs to be verified by further studies using high-resolution regional climate models with detailed aerosol-cloud microphysics.

4. Conclusions

In this work, using model outputs from CMIP5 historical (1870-2005) simulations we have investigated the roles of GHG warming and aerosols on changes in the large-scale circulation structure and rainfall characteristics in Asian monsoon regions. The GHG experiments, which included anthropogenic GHG emissions only is used to establish the base line for assessing ASM climate change. The All experiments, which included additional anthropogenic aerosol emissions is used to evaluate additional aerosol impacts. Results show that under GHG warming, a strong increase in land-sea thermal contrast associated with the Warm-Ocean-Warmer-Land (WOWL) effect spurs a strong increase in anomalous low-level moist static energy (MSE). However, the expansion of the anomalous subsidence zones of the Walker and Hadley Circulations associated with the Deep Tropical Squeeze (DTS), results in extensive regions of anomalous mid-tropospheric dryness over subtropical and mid-latitude land and the Maritime Continent forming a convective barrier (MCB), suppressing ASM convection. Deep convection, strong ascent and heavy rain can only break out in regions where the strong LMSE, facilitated by local processes such as orographic forcing and dynamical feedback, can overcome the MCB.

299 Anthropogenic aerosol emission induces cooling over monsoon land and ocean, masking
300 up to 50% or more of the WOWL effect. As a result, MSE only increases moderately over
301 land, compared to GHG only. The MCB over ASM land region is increased by absorbing
302 aerosols via the semi-direct effect, which increased atmospheric stability and suppress
303 convection [Fan et al. 2008, Lau et al. 2008, 2016, Wang et al., 2013]. Under the combined
304 effects of GHG and aerosols, the overall Asian monsoon circulation is weakened and ASM
305 rainfall reduced. Changes of the monsoon circulation structure, rainfall characteristics,
306 and key remote and regional drivers are shown schematically in Fig. 6. A rainfall scale
307 analysis shows a strong reduction in precipitation efficiency under GHG, reflected in
308 widespread suppressed moderate precipitation, but enhanced extreme heavy
309 precipitation. Under ALL, extreme heavy rain is suppressed, but moderate rain is
310 enhanced over the ASM domain due to the increased lapse-rate stability by absorbing
311 aerosol, in good agreement with rainfall observations from APHRODITE.
312 As a caveat, we should point out that the CMIP5 multi-model mean quantities we
313 examined are only moderately robust, with only approximately 60% of model consistency
314 over the ASM domain. Further work will be needed using "observational constraints" to
315 reduce diversity of model results, and to improve understanding of the underlying
316 physical feedback processes, and skills of ensemble model climate projections [Allen et al.
317 2002]. Most important, our results suggest that the recent debate on whether the ASM is
318 "weakened" or "strengthened" by greenhouse warming or aerosol is not very meaningful.
319 Such a debate is based on the assumption that the underlying circulation structure and
320 rainfall characteristics are unchanged. As demonstrated by our results, this is not the case.
321 Under global warming, competing influences of increased LMSE and large-scale mid-

tropospheric MCB are already set up as a result of planetary scale thermodynamic and dynamical adjustment processes, resulting in changing structure of the ASM meridional circulation and rainfall characteristics. Including anthropogenic aerosol emissions, can further upset the ASM energy and water balance, leading to further changes in circulation and rainfall properties. Indeed, many recent studies have indicated that absorbing aerosols such as desert dusts, black carbon and organic carbon, which are plentiful in the ASM regions, could strengthen the early phase of the ASM via radiation-dynamical feedback processes [Lau et al. 2006, 2008 and others], and that aerosol-cloud microphysics may strongly impact the development of monsoon convection and rainfall [Rosenfeld et al. 2014, and Li et al. 2017]. These aspects of aerosol-monsoon interactions involve both natural and anthropogenic aerosols, and are not considered here. Future work along these lines of investigations will yield further new insights into the fundamental physical processes driving climate change in ASM regions.

Declarations

List of Abbreviations

ALL All forcing including anthrogencic GHG and aerosol emissions

APHRODITE Asian Precipitation Highly-Resolved Observational Data Integration Towards Evaluation

ASM Asian Summer Monsoon

CAPE Convective Available Potential Energy

CMIP5 Coupled Model Intercomparison Project - 5

DTS Deep Tropical Squeeze

GHG Greenhouse Gases

HC Hadley Circulation

ITCZ Inter-Tropical Convergence Zone

MCB Mid-tropospheric Convective Barrier

MMC Monsoon Meridional Circulation

MMM Multi-Model Mean

MSE Moist Static Energy

WC Walker Circulation

WOWL Warm-Ocean-Warmer-Land

Availability of data and materials

CMIP5 model data used for this research are open source data available at data portal http://cmip-pcmdi.llnl.gov/cmip5/data_portal.html. APHRODITE daily precipitation datasets are available from https://climatedataguide.ucar.edu/climate-data

Data for specific analyses and findings are archived in local data repositories at U. of Maryland, and are available upon request.

Competing interests

N/A

Funding

Contract DE-AC05-76RLO1830, Pacific Northwest National Laboratory, Battelle Memorial Institute under the U.S. Department of Energy Office of Science Biological and Environmental Research, Regional and Global Climate Modeling Program. Partial support under Grant# 80NSSC17K0213 was provided by the Modeling Analysis Program (MAP), NASA Headquarters.

Authors' contributions

William K. M. Lau conceived the research, interpreted the results, and wrote the paper. Kyu-Myong Kim conducted the data processing and analyses, and plotted the figures. Ruby Leung provided useful advice and insights on interpretation of results, proof-read and suggested valuable revisions on the final draft of the paper.

Acknowledgement

N/A

Authors' Information

WKM Lau is a senior scientist at the Earth System Science Interdisciplinary Center (ESSIC), adjunct professor at the Department of Atmospheric and Oceanic Sciences, University of Maryland, and former President, Atmosphere Section, American Geophysical Union. During the opening ceremony of the AOGS (Asian Oceania Geophysical Sciences) Meeting, 2017, Singapore, he delivered the Axford Lecture, " *Competing Influences of Greenhouse Warming and Aerosols on Asian Monsoon Climate Change*" which included among other materials, new findings described in this paper.

Figure Captions

Figure 1 Upper panels showing spatial distribution of anomalous 500 hPa negative p-velocity (hPa s^{-1}) for a) GHG only and b) ALL. Contours indicate pre-industrial climatology, with positive (warm color) and negative (blue color) values indicating ascending and descending motions respectively. Grid points where 12 or more out of 19 models agree in the sign of the anomaly are indicated by back circles. Lower panels showing time series (1870-2005) of negative p-velocity averaged over a) the DTS domain (rectangle outlined red), and b) the AMS domain (rectangle outlined black), for GHG (red line) and ALL (blue line) respectively. Thick lines indicate 5- year running mean.

Figure 2 Time series (1870-2005) of ASM domain-averaged anomalies of a) 850hPa MSE, and b) 400 hPa RH. Solid red (blue) lines indicated 5-year running means for GHG (ALL).

Figure 3 Left two panels showing a) latitude-height cross-sections of anomalous negative p-velocity under GHG-only forcing, and b) latitude profiles of anomalies of rainfall (histogram) in mm day^{-1}(left ordinate), 850 hPa MSE (green line) in kJ (right ordinate), and 400 hPa RH (purple line) in percentage (right ordinate). Contours represent climatology. Left two panels c) and d) are the same as a) and b), except for ALL. White dots indicate gridpoints where 12 or more out of the 19 models agree in the sign of the anomaly.

Figure 4 Time series (1870-2005) showing fractional change of precipitation (dP/P), 500 hPa vertical motion (dW/W), moisture (dq/q) and precipitation efficiency ($d\alpha/\alpha$) over the ASM domain for a) GHG and b) ALL.

406 Figure 5 Quantile regression showing trends in fractional change in frequency of rainfall as a
407 function of ranked rain rate for a) GHG only, b) All and c) APHRODITE rainfall
408 observation, for the period 1950-2005. In a) and b), open (solid) circle annotating each
409 quantile represents 10 (12) out of 19 models having the same sign. In c) solid circle
410 represents 95% statistical significance.
411

412 Figure 6 Schematics showing structural changes in the Asian summer monsoon
413 meridional circulation (MMC), rainfall and cloud processes, as a result of
414 competing influences of enhanced low level moisture static energy (MSE) and the
415 mid-tropospheric convective barrier (MCB, denoted by dashed brown line) due to
416 tropospheric drying ($\Delta RH<0$), stemming from adjustment of the large-scale
417 circulation to the Deep Tropical Squeeze (DTS), and regional precipitation-cloud-
418 radiation-dynamical feedback processes under a) GHG warming, and b) combined
419 GHG and aerosol effects. Solid circles denote changes in the oceanic and adjacent-
420 land portion of the MMC. Dashed circles represent anomalous multi-cellular
421 structure over the ASM land regions.
422
423

Reference

Allen MR, Ingram WJ, & Stainforth DA (2002) Constraints on future changes in climate and the hydrologic cycle. Nature 419 (6903), 224.

Ashfaq MD, Rastogi R, Mei D. Touma, Leung LR (2016) Sources of errors in the simulations of south Asian summer monsoon in the CMIP5 GCMs. Clim. Dyn. doi:10.1007/s00382-016-3337-7.

Bollasina M, Ming Y, Ramaswamy V (2011) Anthropogenic aerosols and the weakening of the South Asian summer monsoon. Science doi:10.1126/science.1204994.

Buchinsky M (1998) Recent advances in quantile regression models: A practical guideline for empirical research. J. Human Resour. 33:88–126.

Chung CE, Ramanathan V (2006) Weakening of north Indian SST gradients and the monsoon rainfall in India and the Sahel. J. Climate 19:2036-2045.

Fan J, Zhang R, Tao WK, Mohr KI (2008) Effects of aerosol optical properties on deep convective clouds and radiative forcing. J. Geophys. Res. doi:10.1029/2007JD009257.

Fasullo J (2012) A mechanism for land-ocean contrast in global monsoon trends in a warming climate. Clim. Dym doi:10.1007/s00382-011-1270-3

Fowler HJ, Blenkinsop S, Tebaldi C (2007) Linking climate change modeling to impacts studies: recent advances in downscaling techniques for hydrological modeling. Int. J. Climatol. 27: 1547–1578.

Held IM, Soden BJ (2006) Robust responses of the hydrological cycle to global warming. J. Climate. 19: 5686–5699.

Hu Y, Zhou C, Liu J (2011) Observation evidence of the poleward expansion of the Hadley Circulation. Adv. Atmos. Sci. 28:33-44.

IPCC (2013) Climate Change 2013: The Physical Science Basis, the contribution of Working Group I to the Fifth Assessment Report of the Intergovernmental Panel on Climate Change, edited by Stocker, T.F., D. Qin, G.-K. Plattner, M. Tignor, S.K. Allen, J. Boschung, A. Nauels, Y. Xia, V. Bex and P.M. Midgley, Cambridge University Press, Cambridge, UK and New York, NY, USA.

Jin Q, Wang C (2017) A revival of Indian summer monsoon rainfall since 2002. Nature Climate Change doi:10/1038/NCLIMATE3348.

Koenker R. (2005) Quantile Regression, *Cambridge University Press,* http://www. cambridge.org/9780521845731

Krishnan R, Sabin TP, Ayantika DC, KitohA, Sugi M, Murakami H, Turner A, Slingo JM, Rajendran K (2013) Will the South Asian monsoon overturning circulation stabilize any further? Clim. Dyn 40:187–211.

Lau KM, Wu HT (2006) Trends in tropical rainfall characteristic, 1979-2003. Int.. J. Climatology 27:979-988.

Lau KM, Kim MK, Kim KM, (2006) Aerosol induced anomalies in the Asian summer monsoon: The role of the Tibetan Plateau. Climate Dynamics 26:855-864.

Lau KM, Ramanathan V, Wu GX, Li Z, Tsay SC, Hsu C, Sikka R, Holben B, Lu D, Tartari G, Chin M, Koudelova P, Chen H, Ma Y, Huang J, Taniguchi K, Zhang R (2008) the Joint Aerosol-Monsoon Experiment: A New Challenge in Monsoon Climate Research. Bull. Am. Meteor. Soc. 89:369-383.

Lau KM, Wu HT (2011) Climatology and changes in tropical oceanic rainfall characteristics inferred from Tropical Rainfall Measuring Mission (TRMM) data (1998–2009), J. Geophys. Res. doi:10.1029/2011JD015827.

Lau KM, and Waliser D (eds) (2012) Intraseasonal Variability in the Atmosphere-Ocean Climate System (2nd Edition), Springler, Praxis, Chichester, UK, 613pp. DOI 10.1007/978-3-642-13914-7

Lau KM, Wu HT, Kim KM (2013) A canonical response in rainfall characteristics to global warming from CMIP5 model projections. Geophys. Res. Lett. doi:10.1002/grl.50420.

Lau KM, Kim KM (2015) Robust responses of the Hadley circulation and global dryness form CMIP5 model CO_2 warming projections. Proc. Natl. Acad. Sci. doi:10.1073/pnas.1418682112.

Lau KM, Kim KM, Shi JJ, Matsui T, Chin M, Tan Q, Peters-Lidard C, Tao WK (2016) Impacts of aerosol–monsoon interaction on rainfall and circulation over Northern India and the Himalaya Foothills. Clim. Dym. doi:10.1007/s00382-016-3430-y.

Lau KM, Kim KM (2017) Competing influences of greenhouse warming and aerosols on Asian summer monsoon circulation and rainfall. Asian Pacific J. Atmos. Sci. doi:10.1007/s13143-017-0033-4

Lee JY, Wang B (2012) Future Change of global monsoon in CMIP5 models. Clim. Dym. doi: 10.1007/s00382-012-1564-0.

Li X, Sui CH, Lau KM (2002) Precipitation Efficiency in the tropical deep convective regime: A 2-D cloud resolving model study. J. Meteor. Soc. Japan 80:205-212.

Li J, Wu Z, Jiang Z, He J (2010) Can Global Warming Strengthen the East Asian Summer Monsoon? J. Climate 23:6696–6705.

Li, X, M. Ting C, Li, and Henderson N (2015), Mechanisms of Asian summer monsoon changes in response to anthropogenic forcing in CMIP5 models, J. Climate , 28 (10), 4107–4125, doi:10.1175/JCLI-D-14-00559.1.

493 Li Z, Lau KM, Ramanathan V, Wu G, Ding Y, Manoj MG, Qian Y, Li J, Zhou T, Fan J, Rosenfeld
494 D, Ming Y, Wang Y, Huang J, Wang B, Xu X, Lee SS, Takemura T, Wang K, Xia X, Yin Y,
495 Zhang H, Guo J, Sugimoto N, Liu J, Yang X (2016) Aerosol and monsoon climate
496 interactions over Asia. Review of Geophys. doi:10.1002/ 2015RG000500.
497 Lu J, Vecchi GA, Reichler T (2007) Expansion of the Hadley cell under global
498 warming. Geophys. Res. Lett. doi:10.1029/2006GL028443.
499 Lu J, Leung LR, Yang Q, Chen G, Collins WD, Li F, Hou ZJ, Feng X (2014) The robust
500 dynamical contribution to precipitation extremes in idealized warming simulations
501 across model resolutions. Geophys. Res. Lett., doi:10.1002/2014GL059532.
502 Meehl GA, Arblaster JM, Collins WD (2008) Effects of black carbon aerosols on the Indian
503 monsoon. J. Climate 21:2869–2882.
504 Menon S, Hansen J, Nazarenko L, Luo Y (2002) Climate effects of black carbon aerosols in China
505 and India. Science doi:10.1126/science.1075159.
506 Murugavel P, Pawar SD, Gopalakrishnan V (2012) Trends of Convective Available Potential
507 Energy over the Indian region and its effect on rainfall. Int. J. Climatol. 32: 1362–1372.
508 O' Gorman P, Schneider T (2009) The physical basis for increase in precipitation extremes in
509 simulations of 21st century climate change. Proc. Natl. Acad. Sci., 106:14773-14777.
510 Ramanathan V, Crutzen PJ, Kiehl JT, Rosenfeld D (2001) Aerosols, climate, and the hydrological
511 cycle. Science doi:10.1126/science.1064034.
512 Ramanathan V, Carmichael G (2008) Global and regional climate changes due to black carbon.
513 Nat. Geosci. doi:10.1038/ngeo156.

514 Ramanathan V, Feng Y (2008) On avoiding dangerous anthropogenic interference of the
515 climate system: Formidable challenges ahead. Proc. Natl. Acad. Sci. doi:
516 10.1073/pnas.0803838105.
517 Rosenfeld D, Andreae MO, Asm, A, Chin M, de Leeuw G, Donovan, DP, Kahn R, Kinne S,
518 Kivekäs N, Kulmala M, Lau WKM, Schmidt S, Suni T, Wagner T, Wild M, Quaas J
519 (2014) Global observations of aerosol-cloud-precipitation-climate interactions. Reviews
520 of Geophysics, DOI 10.1002/2013RG000441.
521 Roxy MK, Ritika K,Terray P, Murtugudde R, Ashok K, Goswami B (2015) Drying of Indian
522 subcontinent by rapid Indian Ocean warming and a weakening land-sea thermal gradient.
523 Nature Communications doi:10.1038/ncomms8423.
524 Santer B et al. (2012) Identifying human influences on atmospheric temperature. Proc. Natl.
525 Acad. Sci doi: 10.1073/pnas.1210514109
526 Seidel DJ, Fu Q, Randel WJ, Reichler TJ (2008) Widening of the tropical belt in a changing
527 climate. Nature Geoscience doi:10.1038/ngeo.2007.38
528 Sherwood SC, Ingram W, Tsushima Y, Satoh M, Roberts M, Vidale PL, O'Gorman PA (2010)
529 Relative humidity changes in a warmer climate. J. Geophys. Res.
530 doi:10.1029/2009JD012585
531 Song F, Zhou T, Qian Y (2014) Responses of East Asian summer monsoon to natural and
532 anthropogenic forcings in the 17 latest CMIP5 models. Geophys. Res. Lett. 41:596–603.
533 Sperber KR, Annamalai H, Kang IS, Kitoh A, Moise A, Turner A, Wang B, Zhou T (2013) The
534 Asian summer monsoon: an intercomparison of CMIP5 vs. CMIP3 simulations of the
535 late 20th century. Clim. Dyn. 41:2711-2744.

536 Sugiyama M, Shiogama H, Emori S (2010) Precipitation extreme changes exceeding moisture
537 content increases in MIROC and IPCC climate models. Proc. Natl. Acad. Sci.
538 U.S.A. 107:571–575.
539 Sui CH, Li X, Yang MJ (2007) On the definition of precipitation efficiency. J. Atmos. Sci. 64:
540 4506-4513.
541 Tokinaga H, Xie SP, Timmermann A (2012) Regional Patterns of Tropical Indo-Pacific Climate
542 Change: Evidence of the Walker Circulation Weakening. J. Climate **2**5:1689- 1709.
543 Trenberth K, Dai A, Rasmussen RM, Parsons DB (2003) The changing character of
544 precipitation. Bull. Am. Meteor. Soc., doi: 10.1175/BAMS-84-9-1205
545 Turner AG, Annamalai H (2012) Climate change and the South Asian summer monsoon. Nature
546 Climate Change doi: 10.1038/NCLIMATE1495.
547 Vecchi GA, Soden BJ (2007) Global Warming and the Weakening of the Tropical Circulation. J.
548 Climate 20:4316–4340.
549 Wang B, Liu J, Kim H, Webster P, Yim S (2012) Recent change of the global monsoon
550 precipitation (1979–2008). Clim Dyn 39:1123–1135.
551 Wang B (2006) *The Asian Monsoon*, Praxis Publishing Ltd., Chichester, UK. 787pp.
552 Wang C, Kim D, Ekman AML, Barth MC, Rasch PJ (2009) Impact of anthropogenic aerosols on
553 Indian summer monsoon. Geophys. Res. Lett. doi:10.1029/2009GL040114.
554 Wang Y, Khalizov A, Levy M, Zhang R (2013) New directions: Light absorbing aerosols and
555 their atmospheric impacts. Atmos. Environ. 81:713–715.
556 Wang Y, Zhou L (2005) Observed trends in extreme precipitation events in China during 1961 –
557 2001 and the associated changes in large-scale circulation. Geophys. Res.Lett.
558 doi:10.1029/2005GL022574.

559 Webster PJ, Magaña VO, Palmer TN, Shukla J, Tomas RA, Yanai M, Yasunari T (1998)
560 Monsoons: Processes, predictability, and the prospects for prediction. J. Geophys. Res.
561 doi:10.1029/97JC02719.
562 Xie SP, Deser C, Vecchi GA, Ma J, Teng J, Wittenberg A (2009) Global warming pattern
563 formation: sea surface temperature and rainfall. J. Climate,
564 https://doi.org/10.1175/2009JCLI3329.1.
565 Yang X, Yao Z, Li Z, Fan T (2013) Heavy air pollution suppresses summer thunderstorms in
566 central China. J. Atmos. Solar-Terrestrial Phys. doi:10.1016/j.jastp.2012.12.023.
567 Yatagai A, Kamiguchi K, Arakawa O, Hamada A, Yasutomi N, Kitoh A (2012) APHRODITE:
568 Constructing a Long-Term Daily Gridded Precipitation Dataset for Asia Based on a
569 Dense Network of Rain Gauges. Bull. Amer. Meteor. Soc. 93:1401–1415.
570 Zhang, L, & Li T (2016) Relative roles of anthropogenic aerosols and greenhouse gases in land
571 and oceanic monsoon changes during past 156 years in CMIP5 models. Geophy.
572 Res. Lett., 43(10), 5295-5301.
573

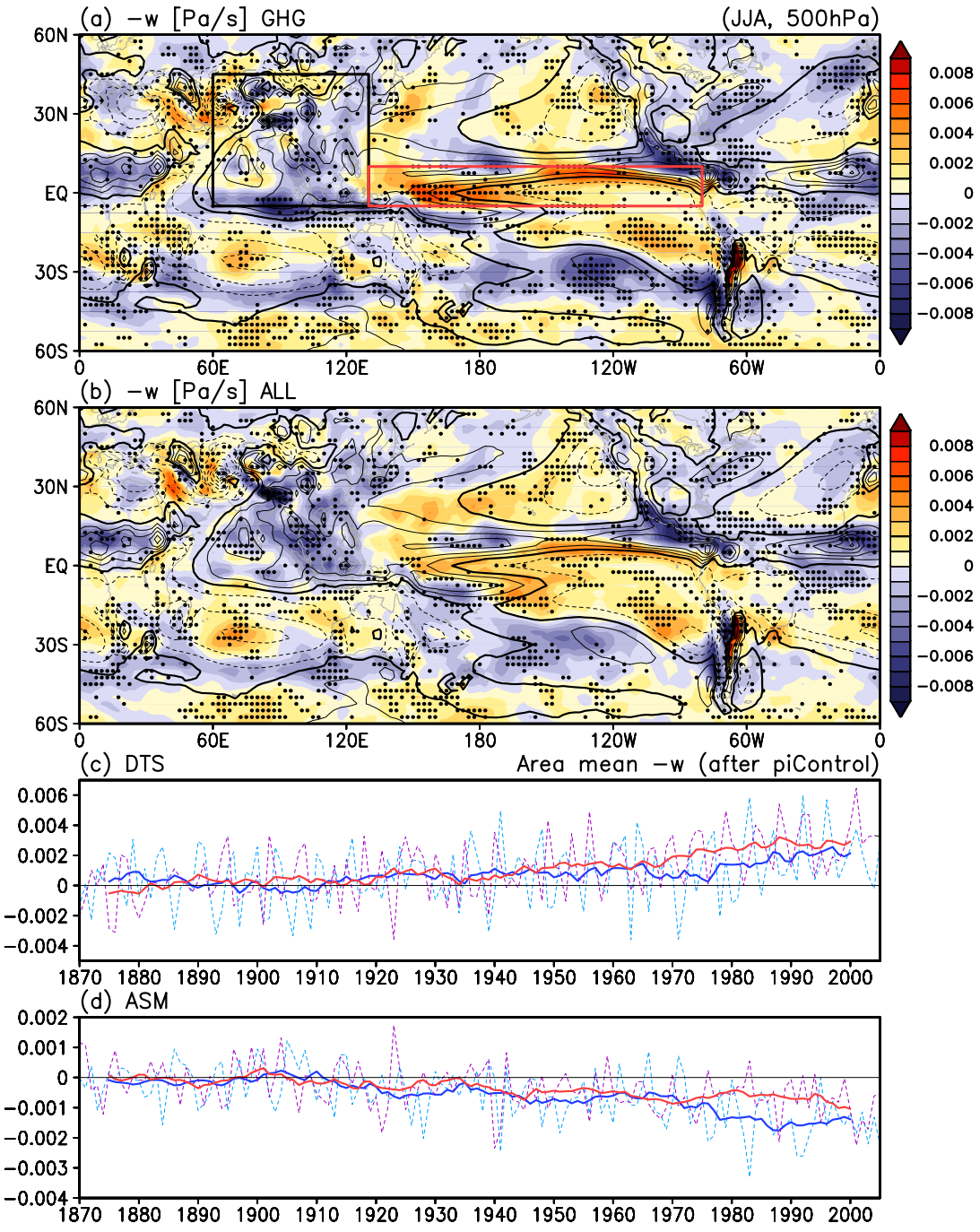

Figure 1 Upper panels showing spatial distribution of anomalous 500 hPa negative p-velocity (hPa s^{-1}) for a) GHG only and b) ALL. Contours indicate PI climatology, with positive values (warm color) and negative values (blue) indicating ascending and descending motions respectively. Grid points where more than 12 out of 19 models agree in the sign of the anomaly are indicated by black circles. Lower panels showing time series (1870-2005) of negative p-velocity averaged over c) the DTS domain (rectangle outlined in red), and d) the AMS domain (square outlined in black), for GHG (red line) and ALL (blue line) respectively. Thick lines indicate 5- year running mean.

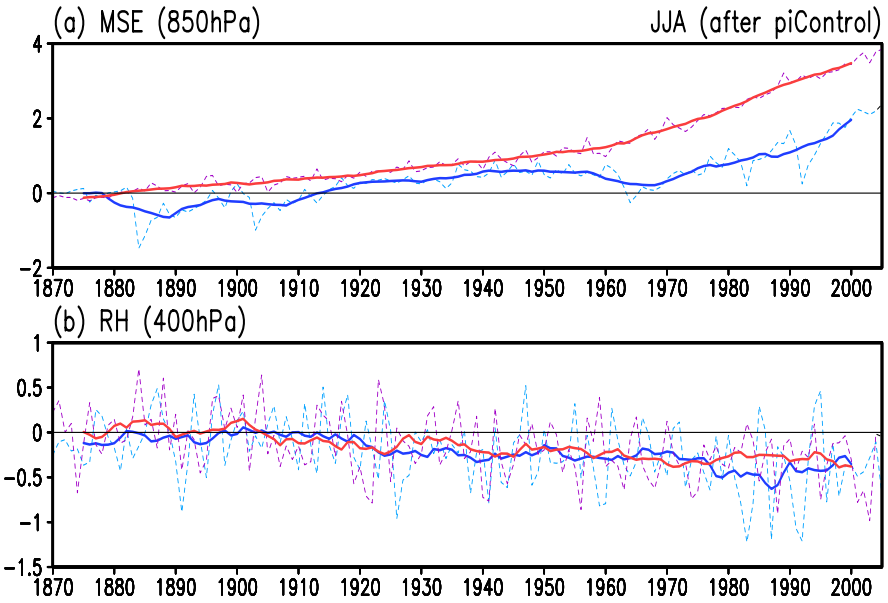

Fig. 2 Time series (1870-2005) of ASM domain-averaged anomalies of a) 850hPa MSE, and b) 400 hPa RH. Solid red (blue) lines indicated 5-year running means for GHG (ALL).

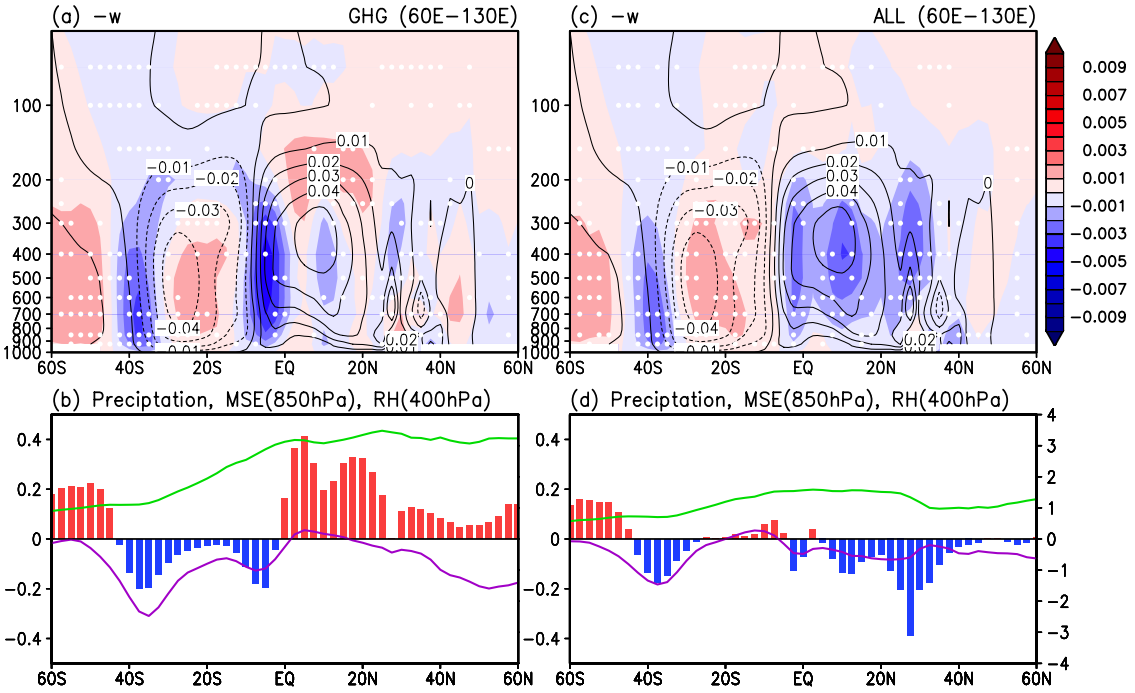

Fig. 3 Left two panels showing a) latitude-height cross-sections of anomalous negative p-velocity and b) latitude profiles of anomalies of rainfall (histogram) in mm day^{-1}(left ordinate), 850 hPa MSE (green line) in kJ (right ordinate), and 400 hPa RH (purple line) in percentage (right ordinate) under GHG-only forcing. Right two panels c) and d) are the same as a) and b), except for ALL. White dots indicate gridpoints where more than 12 out of the 19 model agree in the sign of the anomaly.

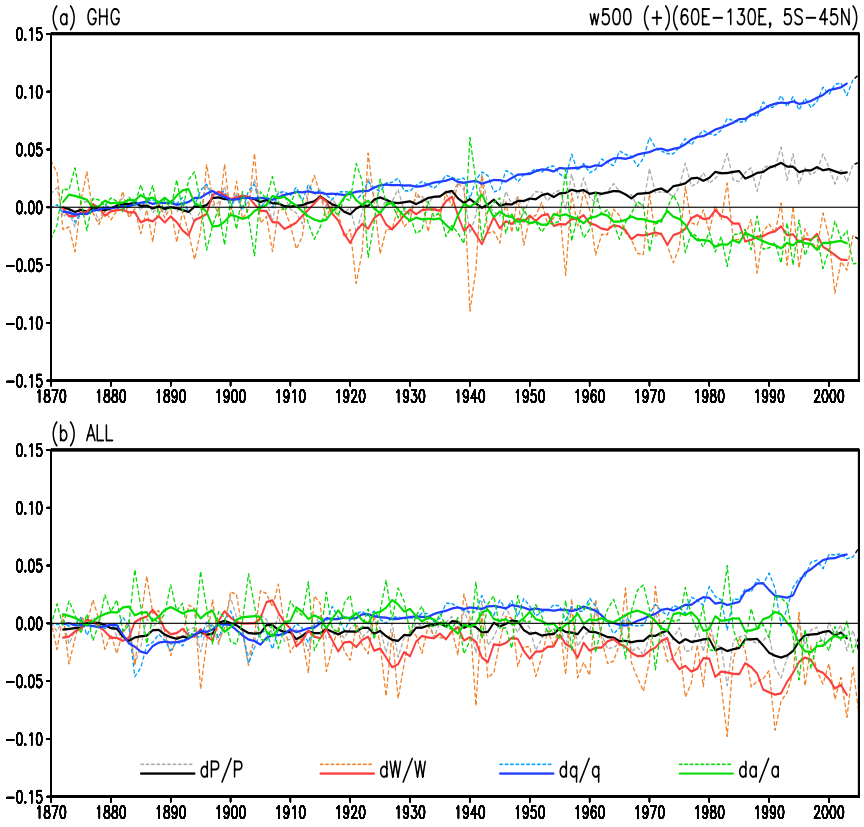

Fig. 4 Time series (1870-2005) showing fractional change of precipitation (dP/P), 500 hPa vertical motion (dW/W), moisture (dq/q) and precipitation efficiency (dα/α) over the ASM domain for a) GHG and b) ALL.

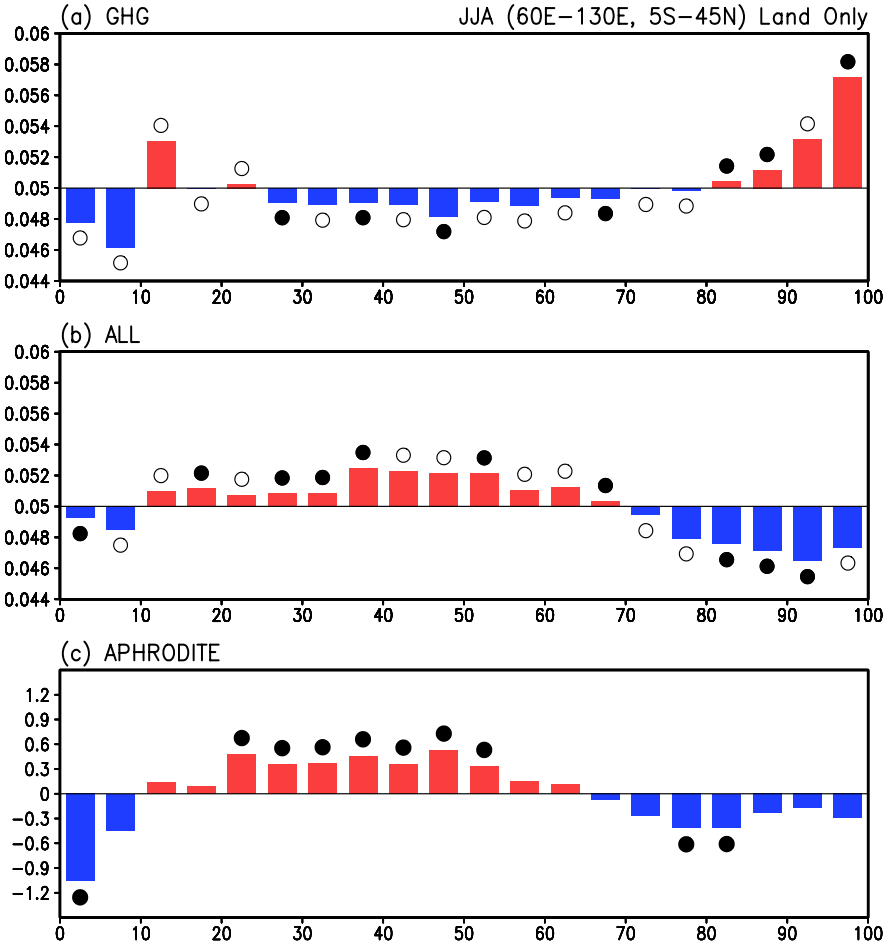

Figure 5 Quantile regression showing trends in fractional change in frequency of rainfall as a function of ranked rain rate for a) GHG only, b) All and c) APHRODITE rainfall observation, for the period 1950-2005. In a) and b), open (solid) circle annotating each quantile represents 10 (12) out of 19 models having the same sign. In c) solid circle represents 95% statistical significance.

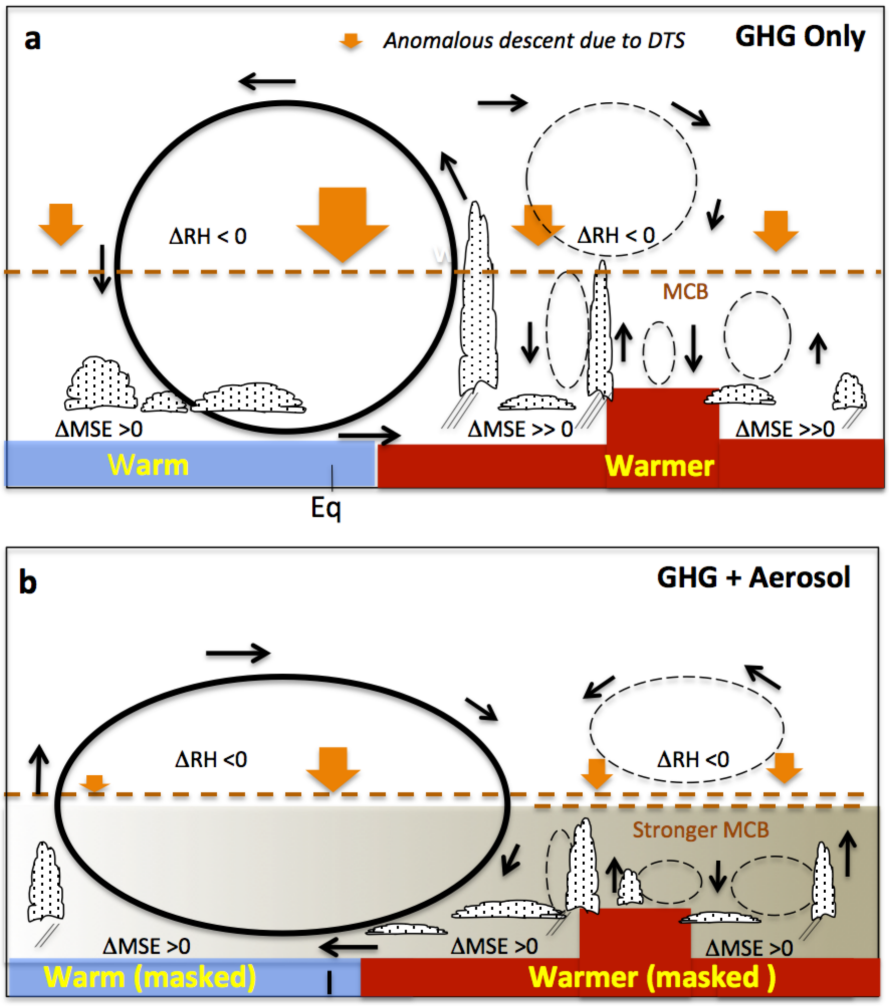

Figure 6 Schematic showing structural changes in the Asian summer monsoon meridional circulation (MMC), rainfall and cloud processes, indicating competing influences of enhanced low level moisture static energy (MSE) and the mid-tropospheric convective barrier (MCB, denoted by dashed brown lines) due to tropospheric drying (ΔRH<0), resulting from adjustment of the large-scale circulation to the Deep Tropical Squeeze (DTS) and regional response and feedback processes under a) GHG warming, and b) combined GHG and aerosol effects. Solid circles denote changes in the oceanic and adjacent-land portion of the MMC. Dashed circles represent anomalous multi-cellular structure over the ASM land regions. In b), stronger MCB due to increased atmospheric stability by aerosols over ASM land is denoted by double dashed brown lines